Eur Biophys J (2012) 41:931–938
DOI 10.1007/s00249-012-0845-1

ORIGINAL PAPER

EBSA
Biophysics in Europe

Amyloid fibril formation from human and bovine serum albumin followed by quasi-simultaneous Fourier-transform infrared (FT-IR) spectroscopy and static light scattering (SLS)

Igor de la Arada · Christian Seiler · Werner Mäntele

Received: 14 May 2012 / Revised: 20 July 2012 / Accepted: 27 July 2012 / Published online: 7 September 2012

Abstract Human and bovine serum albumins are widely known proteins that can form amyloid fibrils under destabilizing conditions. Use of well-known proteins with easily-controlled aggregation process, and comparison of these processes for similar proteins from different species, could help elucidate the nature of the aggregation process implicated in many degenerative diseases, for example Alzheimer's, Parkinson's, or type II diabetes. In this work both amyloidogenic mechanisms have been studied by use of infrared spectroscopy in combination with static light scattering, enabling analysis of intra and intermolecular processes and measurement of prefibril and fibril growing quasi-simultaneously. Deeper insight into the rearrangements of the secondary structure of the proteins concomitant with the aggregation process has also been gained by mathematical analysis of the infrared spectra by two-dimensional correlation spectroscopy (2DCOS).

Keywords Amyloid · Fourier-transform infrared (FT-IR) spectroscopy · Static light scattering (SLS) · Two-dimensional correlation spectroscopy (2DCOS) · Bovine serum albumin (BSA) · Human serum albumin (HSA)

I. de la Arada (✉) · C. Seiler · W. Mäntele
Institut für Biophysik, Goethe-Universität Frankfurt,
Max-von-Laue-Straße 1, 60438 Frankfurt am Main, Germany
e-mail: igor.delaarada@ehu.es

Present Address:
I. de la Arada
Dpto. Bioquímica y Biología Molecular (UPV/EHU),
Unidad de Biofísica (CSIC-UPV/EHU), P.O. Box 644,
48080 Bilbao, Spain

Introduction

Protein misfolding and formation of amyloid fibrils are associated with human diseases including Alzheimer's, Parkinson's, and type II diabetes (Chiti and Dobson 2006), but the occurrence of these highly ordered aggregates has been observed not only in disease-related proteins but also in apparently nonpathogenic species, indicating they could be a conformational state for all polypeptide chains (Dobson 2003). Moreover, these nonpathogenic fibrils have morphological and structural properties similar to those of the pathogenic type (Tycko 2004), suggesting a common mechanism in the fibrillation pathway that originates from the so-called cross-β structure (Bucciantini et al. 2002). There is currently no promising therapy for amyloid-related diseases. Thus, the study of amyloid fibril formation is an active area of research for pathogenic amyloid aggregates that are related with diseases. The study of proteins that can form amyloid-like structures in vitro but are not related with any disease is equally relevant (Chiti and Dobson 2006; Jahn and Radford 2008; Kumar and Udgaonkar 2010).

Infrared spectroscopy has been extensively used to follow amyloid formation (de la Arada et al. 2011; Bouchard et al. 2000; Cerdà-Costa et al. 2009; Termine et al. 1972). Coupled with two-dimensional correlation analysis (2DCOS) (Noda 2007) it enables more detailed analysis of secondary structure conversion from the initial monomer to the amyloid fibril. The information obtained from IR spectroscopy is, however, local, and is limited to the structural properties of the individual protein and to the interfacial regions of contact that are relevant for fibril formation. To gain better insight into the amyloidogenic process, a static light scattering (SLS) system has been coupled in situ with an infrared spectrometer. Static light scattering, in contrast with IR spectroscopy, can monitor

size evolution in the range from 1 to 1,000 nm and is thus sensitive to the aggregation process and fibril formation. Integration of an SLS system in the FT-IR spectrometer facilitates quasi-simultaneous measurement of local structural changes together with larger-range size alterations, using the same sample and identical conditions.

In this work, one and two-dimensional IR correlation spectroscopy and SLS have been used to study the formation of amyloid fibrils from human and bovine serum albumin.

Materials and methods

Materials

Human serum albumin (HSA) and bovine serum albumin (BSA) were purchased from Sigma–Aldrich (St Louis, MO, USA). Hepes buffer, NaCl, KCl, and $CaCl_2$ were purchased from Carl Roth (Karlsruhe, Germany) and deuterium oxide (D_2O) was obtained from Euriso-Top (Gif sur Yvette, France).

BSA and HSA fibril formation

To initiate the formation of BSA or HSA amyloid-like fibrils, the proteins were incubated at 80 °C and pD 7.4 (pD = pH + 0.4 units) (Lumry et al. 1951) in deuterated Hepes buffer (40 mM Hepes, 60 mM NaCl, 4 mM KCl, 3.3 mM $CaCl_2$). Typical protein sample concentration was 1.5 mM.

Fourier-transform infrared spectroscopy (FT-IR)

For FT-IR measurements approximately 1 µl sample containing 1.5 mM protein solution in deuterated Hepes buffer was loaded between two flat CaF_2 windows with a pathlength of 20 µm (Fabian et al. 2002). To avoid drying of the sample, the windows were sealed with PTFE paste (Carl Roth, Karlsruhe, Germany) and loaded into a thermostated sample holder. Typically 70 scans were collected for the background and the sample by using OPUS software in a Bruker Vector 22 FT-IR spectrometer equipped with a DTGS detector (Bruker Optik, Ettlingen, Germany). The spectrometer was also equipped with a sample shuttle that automatically moves the sample holder from the "sample position", where the infrared beam passes through the sample, to the "background position" in which the infrared beam passes directly to the detector. This single-beam spectrum was used as the background spectrum. Both sample and background spectrum were obtained with a nominal resolution of 2 cm^{-1}. Data treatment has been described elsewhere (Arrondo et al. 1993).

To obtain the 2DCOS infrared maps, the incubation time of the protein sample at 80 °C was used as the perturbation to induce spectral fluctuations and to detect dynamic spectra arising from variation of the secondary structure of the different samples. To generate the 2DCOS maps, Kinetics software for Matlab developed by Erik Goormaghtigh from the Université Libre de Bruxelles was used (Raussens et al. 2004). Correlation between bands is found via the so-called synchronous and asynchronous spectra that correspond to the real and imaginary parts of the cross-correlation of spectral intensity at two wavenumbers. In a synchronous 2DCOS map, the peaks located in the diagonal (termed "autopeaks") correspond to changes in intensity induced by the external perturbation, and are always positive. The cross-correlation peaks indicate an in-phase relationship between the two bands involved. Asynchronous maps show out-of-phase cross-correlation between the bands. This provides information not only about the interaction among bands, but also about the time-course of the events caused by the perturbation.

Static light scattering

A specially developed light-scattering apparatus (Fig. 1) was used for the measurements. Samples, CaF_2 windows, and thermostated cell holder were the same as for the FT-IR measurements. The sample was irradiated with a light beam from a light-emitting diode (LED) (λ_{max} 445 nm) attached to a thermostated copper heat sink to minimize intensity fluctuation and drift. An optical fiber was used to direct the light from the LED to the cell holder. A collimator at the end of the optical fiber was used to obtain parallel light. The scattered light in the forward direction

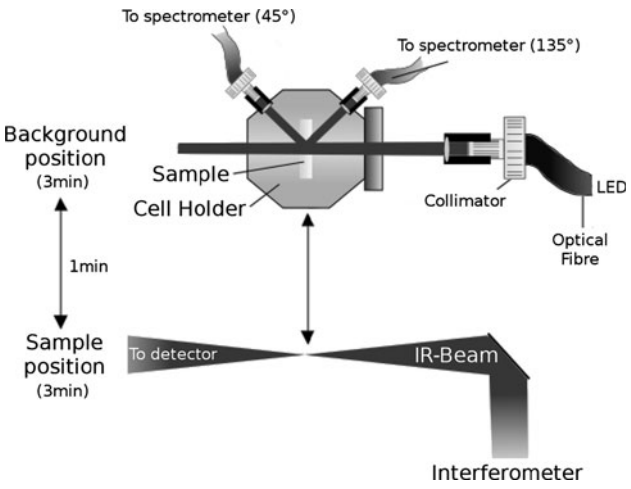

Fig. 1 Schematic representation of the infrared spectrometer coupled with the light-scattering device. The sample moves automatically every 3 min from the background position to sample position, enabling FT-IR and SLS measurements

(at 45°) and backscattered light (at 135° to the forward direction) was collected by further fiber collimators, and sent to a two different USB4000 spectrometers (Ocean Optics, Dunedin, FL, USA) one for each angle. When the cell holder was in the FT-IR background measurement position, the light scattering integral intensities were recorded by use of the software suite from Ocean Optics.

Results

Structural changes during BSA and HSA fibril formation

Human serum albumin (HSA), bovine serum albumin (BSA), and other albumins have been reported to form amyloid fibrils in vitro (Juárez et al. 2009; Militello et al. 2004; Pearce et al. 2007). Although they are not predisposed to form this kind of aggregate, because of the lack of properties that suggest this predisposition and their high α-helix structure content, there are conditions that favor partly destabilized monomers and dimers, for example low pH, high temperatures, or the presence of chemical denaturants, that can force amyloidogenesis (Gorinstein et al. 2002). For the analysis reported here, we induced amyloid fibril formation by use of high temperatures while maintaining neutral pH.

Figure 2 shows FT-IR spectra of HSA and BSA obtained after incubation for different times. This figure demonstrates the temperature-dependent changes that occur during incubation. Initially, a prominent high-intensity band centered at approximately 1,654 cm^{-1} is observed for both albumins. This band can be assigned to the amide I′ modes of these predominantly alpha helical proteins (Arrondo et al. 1993). With increasing incubation time, the intensity of this band is reduced and two new bands, centered at 1,615 and 1,684 cm^{-1}, appear and continue to grow. These bands arise from interchain beta-sheet-type hydrogen bonds related to the amyloidogenic structure (Zurdo et al. 2001). These are the most marked changes that appear during the amyloidogenesis of both albumins.

To analyze the differences between the beginning and end of the process for both proteins, difference spectra were obtained by subtraction of BSA and HSA spectra acquired after incubation for 0 and 200 min (Fig. 3). From the flat shape of the difference spectrum it is clearly apparent the amide I′ bands of both proteins are similar at the beginning of the incubation. The slight differences are because of the lower intensity of the maximum at 1,654 cm^{-1} for bovine albumin (Fig. 3a). The differences become much more evident at the end of the incubation. The positive band centered at 1,654 cm^{-1} is indicative of more residual helicoid structure in bovine albumin. On the other hand, the negative signal in the difference spectra at 1,615 cm^{-1} reflects lower aggregation of BSA compared with HSA. These results indicate a different final structure of the aggregates obtained, although they are initiated from a very similar structure.

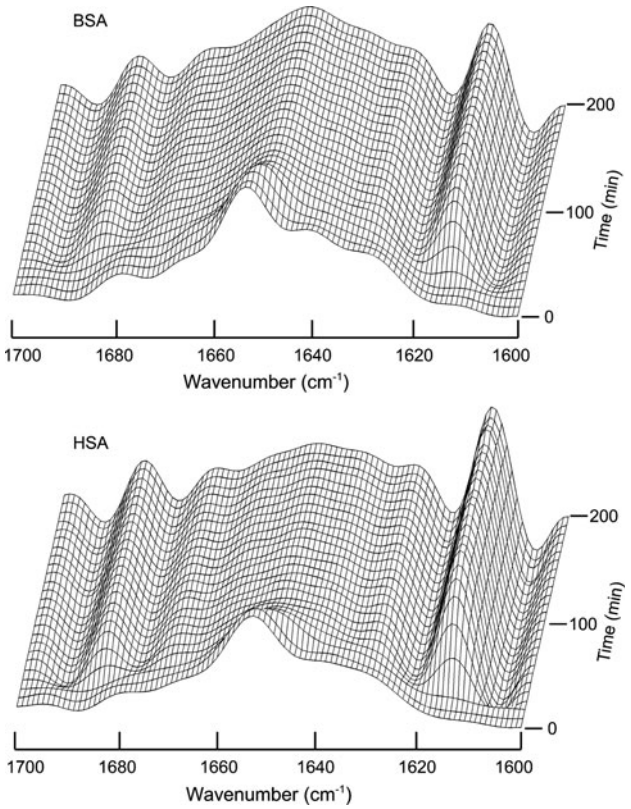

Fig. 2 Three-dimensional plot of deconvolved FT-IR spectra (half width = 18 and $K = 2$) of BSA (*top*) and HSA (*bottom*) recorded at 80 °C

Two-dimensional correlation analysis

To analyze whether the amyloidogenic process is also different for both albumins, we applied 2D correlation analysis to the infrared spectra. On the basis of the broad autopeaks and their correlations in the synchronous (Φ) 2DCOS maps (Fig. 4, left), we conclude there are no big differences between the proteins. In both maps, two intense autopeaks are detected, one at 1,654 cm^{-1}, typically attributed to α-helical content, and the other at 1,615 cm^{-1}, arising from inter-molecular β-sheet structures with strong hydrogen bonds, usually found in amyloid structures. These autopeaks are correlated by an equally intense negative cross-peak indicating that one of the bands increases in intensity (1,615 cm^{-1}, as we have seen previously) whereas the other decreases (1,654 cm^{-1}). There is another autopeak in the BSA synchronous map, related to anti-parallel inter-molecular β-sheet aggregates (1,684 cm^{-1}),

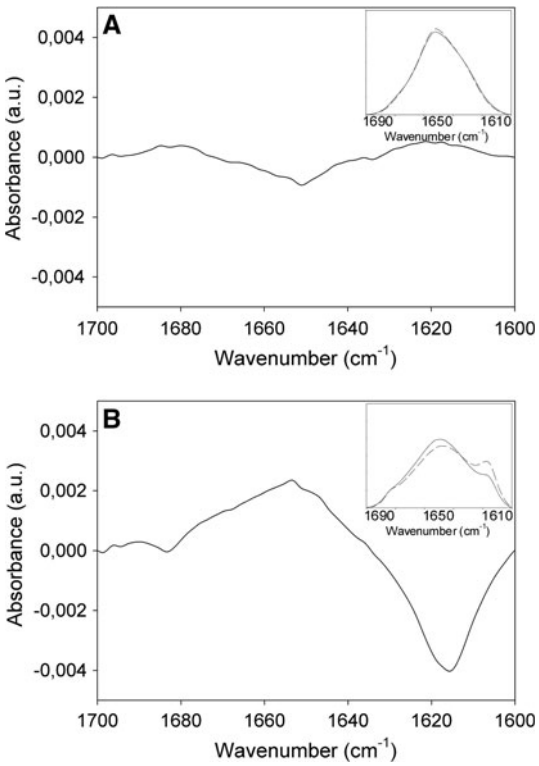

Fig. 3 Differential infrared spectra of the amide I′ band of BSA and HSA at 25 °C (**a**) and 80 °C (**b**) after incubation for 200 min. The original spectra of BSA (*solid line*) and HSA (*dashed line*) are shown in the *insets*

that it is missing in the HSA synchronous map. Although this autopeak is not present in one of the maps, we can observe cross-peaks that correlate the 1,684 cm^{-1} autopeak with the other two in the BSA and HSA maps. These correlations are similar for both maps, negative for the correlation with the helicoid-content autopeak (1,654 cm^{-1}) and positive for the other. This reaffirms that the process is mainly driven by an increase of the components related to the fibril at the expense of the reduction of the native α-helix structure of the proteins.

More information about the time of events can be extracted from the asynchronous (Ψ) maps (Fig. 4 right). A first glimpse at this map confirms that the kinetics of fibril formation are slightly different for human and bovine albumins, with different correlation peaks (Table 1). The time-course of the events can be followed by studying the intensity and sign of the peaks. If the cross-correlated peak is positive, the correlated position on the *x*-axis starts to change before that on the *y*-axis, and in the opposite way if it is negative. Nevertheless, this rule is reversed when superimposing the asynchronous peak on the synchronous map—the peak is placed in a negative area of this map (Noda's rule) (Noda and Ozaki 2004). Following Noda's rule, a positive asynchronous peak becomes negative, or a negative one becomes positive, if the synchronous correlation intensity at the same coordinates is negative. In Table 1 we show the signs of the peaks, the sign of the same area in the synchronous map, and the order of the event.

The peaks in the asynchronous maps correlate six bands that can be assigned to inter-molecular β-sheets (1,615 cm^{-1}), unordered structures (1,648 cm^{-1}), turns (1,670 cm^{-1}), α-helix structures (1,654 cm^{-1}), and antiparallel inter-molecular β-sheets (1,684 cm^{-1}). The band at 1,628 cm^{-1} is usually assigned to β-sheet structures (Arrondo et al. 1993) and it has also been assigned to this structure in HSA (Bramanti and Benedetti 1996; Charbonneau et al. 2009; Froehlich et al. 2009), although X-ray diffraction experiments with HSA shows only α-helix, extended polypeptide, and turn structures (He and Carter 1992; Sugio et al. 1999). This contradiction suggests that the 1,628 cm^{-1} band in the IR spectrum could be the contribution of both extended chain and β-sheet structures (Huang et al. 2011).

Looking at the correlated peaks of both albumins we find that seven out of nine peaks are similar. The similar peaks correspond to the correlations between the amyloid-related bands (1,615 and 1,684 cm^{-1}) with turns (1,670 cm^{-1}), unordered structures (1,648 cm^{-1}), and the extended chain and β-sheet structures (1,628 cm^{-1}). In both cases the unordered structures and the extended chain/β-sheet structures start to change before the amyloid related structures, and the turns change subsequently. Other similarities found in the asynchronous maps are the peaks correlating α-helix (1,654 cm^{-1}) with unordered structures (1,648 cm^{-1}) and turns (1,670 cm^{-1}), with the changes starting in the less ordered structures before those in the α-helix.

Apart from these similarities there are two different peaks in BSA and HSA maps. In the BSA map, the band assigned to helicoid structures (1,654 cm^{-1}) and to the antiparallel inter-molecular β-sheets of the fibril (1,684 cm^{-1}) correlate with the band related to the extended chain/β-sheet structures (1,628 cm^{-1}), whereas in the HSA map these correlations are with the band assigned to the inter-molecular β-sheets of the amyloid structure (1,615 cm^{-1}). Nevertheless the order of events is the same, with the changes starting in the α-helix and then in the antiparallel inter-molecular β-sheets afterwards.

Although the correlation peaks are not exactly the same for both proteins, as judged from the peak signs, the molecular events characterized by the maxima of the bands observed during the time course are very similar for both albumins:

BSA: 1,648 cm^{-1}/1,628 cm^{-1} → 1,615 cm^{-1}/1,684 cm^{-1} → 1,670 cm^{-1} → 1,654 cm^{-1}

HSA: 1,648 cm^{-1}/1,628 cm^{-1} → 1,615 cm^{-1} → 1,684 cm^{-1} → 1,670 cm^{-1} → 1,654 cm^{-1}

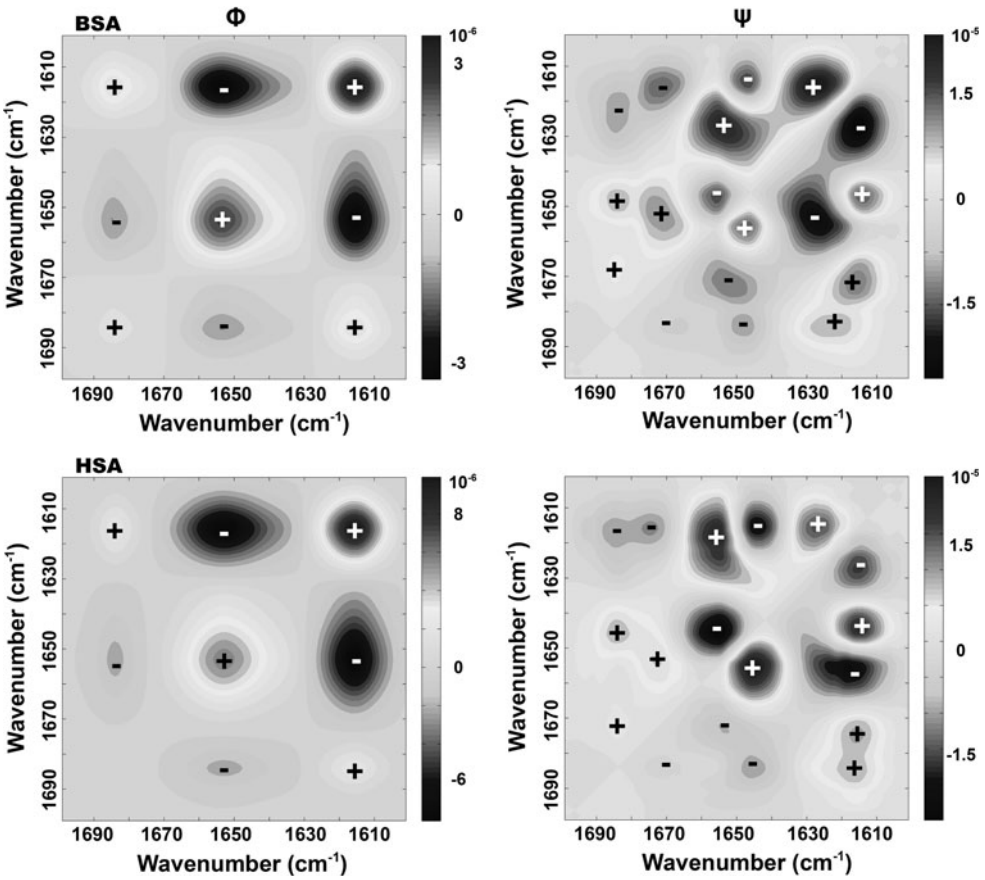

Fig. 4 Synchronous (Φ) and asynchronous (Ψ) 2DCOS maps of BSA (*top*) and HSA (*bottom*) corresponding to the amide I′ band using temperature as the external perturbation. The sign of the peaks has been marked with a *positive sign* for the positive correlations and with a *negative sign* for the negative correlations

Table 1 Summary of correlated peaks observed in the lower right section of the asynchronous map

BSA asynchronous correlated peaks				HSA asynchronous correlated peaks			
Pairs	Sign	Area (Φ)	Order of event	Pairs	Sign	Area [Φ]	Order of event
1,615/1,670	+	+	→	1,615/1,684	+	+	→
1,615/1,648	+	−	←	1,615/1,670	+	+	→
1,615/1,628	−	+	←	1,615/1,654	−	−	→
1,628/1,684	+	+	→	1,615/1,648	+	−	←
1,628/1,654	−	−	→	1,615/1,628	−	+	←
1,648/1,684	−	−	→	1,648/1,684	−	−	→
1,648/1,654	+	+	→	1,648/1,654	+	+	→
1,654/1,670	−	+	←	1,654/1,670	−	+	←
1,670/1,684	−	+	←	1,670/1,684	−	+	←

The sign of the peak in the asynchronous map ("Sign"), the sign of the same area in the synchronous map ("Area (Φ)"), and the order of event are shown

These spectral signatures can be converted into sequences of molecular events. There is a first major change in the unordered structure of the albumins (1,648 cm^{-1}). Then the bands related to the fibril (1,615 and 1,684 cm^{-1}) start to change, followed by changes in the flexible structures (1,670 cm^{-1}) with an subsequent rearrangement of the helical content (1,654 cm^{-1}).

Quasi-simultaneous static light scattering (SLS) and FT-IR measurement

Light scattering has already been used to analyze fibril formation by some proteins (Hill et al. 2011; Militello et al. 2004; Witte et al. 2007). As far as we are aware, however, no studies have combined SLS and FT-IR under identical

conditions and for the same sample. For the FT-IR experiments, because of the high absorbance of aqueous solutions in the amide I region, it is necessary to use a very small path length of ca 5–50 μm. Consequently, the protein concentration must be relatively high (100 μM to some mM). Light scattering is normally monitored for much more dilute suspensions, but with much larger pathlengths (∼cm) compared with IR spectroscopy. Comparison of amyloid fibril formation followed by these different techniques would bear the risk that the processes are not comparable, in particular because of the effect of protein concentration on aggregation. We thus chose to use a coupled device to follow the amyloidogenic process on the same sample, at the same path length, and under identical temperature and pH conditions for both techniques in a quasi-simultaneous measurement.

In static light scattering, the size, d, of scattering objects relative to the wavelength, λ, of the scattered light has an important effect on physical description of the process, i.e., the angular dependence of the scattered light intensity $I(\Theta)$. For very small particles ($d \ll \lambda$), classical dipolar Rayleigh scattering theory can be used. As particle size increases ($d < \lambda$) or even comes close to the wavelength ($d \cong \lambda$), Rayleigh–Gans–Debye scattering theory applies. For even larger particles, Mie scattering or Fraunhofer scattering theory must be used (van de Hulst 1981). If visible light is used for excitation of static light scattering and a particle size from some nm to some 100 nm is considered, Rayleigh or Rayleigh–Gans–Debye theory can be used to describe the scattering intensities $I(\Theta)$. However, it should be mentioned that scattering theories have been developed for spherical particles and for simple geometric forms (discs, cylinders), and that long, irregular, and eventually bent or twisted fibers, for example amyloid fibrils, are difficult to describe quantitatively. We will thus use light scattering intensities at two angles (45° and 135°) for qualitative description, only, of the number of scattering particles by following the intensity at 45°, and for coarse description of the increase in size by following the dissymmetry ratio $I_{45°}/I_{135°}$ (Wyatt 1993).

The increase in the intensity of the scattered light with amyloidogenesis (Fig. 5) occurs in a concerted way in both forward (45°) and backward (135°) scattering. As can be seen from the time profile of the low-frequency FT-IR band at 1,615 cm^{-1} related to the fibril (Fig. 5d), the overall rate of aggregation is faster for human albumin. The time-dependence of the FT-IR spectra (Figs. 2 and 5) reveals half-times are of the order of 38 and 27 min for BSA and HSA, respectively, whereas the simultaneously recorded light-scattering signals indicate half-times are 48 and 25 min. These differences can be explained on the basis of the different information provided by the techniques. Whereas FT-IR signals arise from local changes of the secondary structure and the interfaces of the protein, the scattered light tells us about the number and size of the scattering particles. For human albumin the increase in the number of particles follows a similar time course to the growth of the band related to the fibril. For BSA, however, the structural changes occur more quickly than the increase in the number of particles (Fig. 6). The maximum of the scattering intensity of HSA is higher than that of BSA, which confirms that the amyloidogenesis is not only faster,

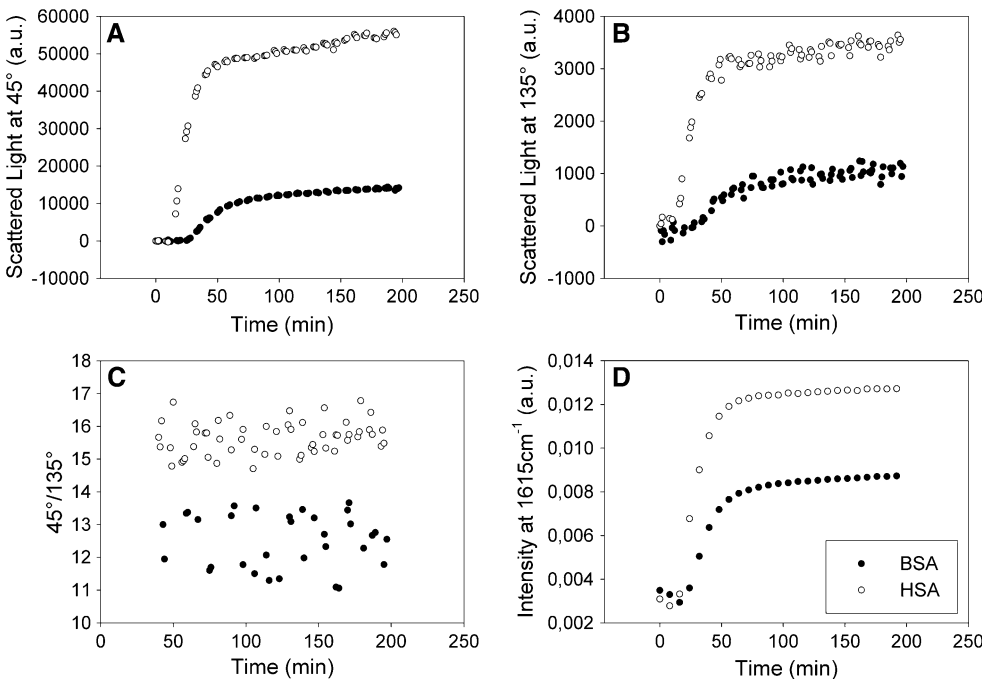

Fig. 5 Light-scattering measurement of BSA and HSA at 45° (**a**) and 135° (**b**). Scattered light ratio 45°/135° between 40 and 200 min during incubation at 80 °C (**c**). Time dependence of the FT-IR band at 1,615 cm^{-1} (**d**)

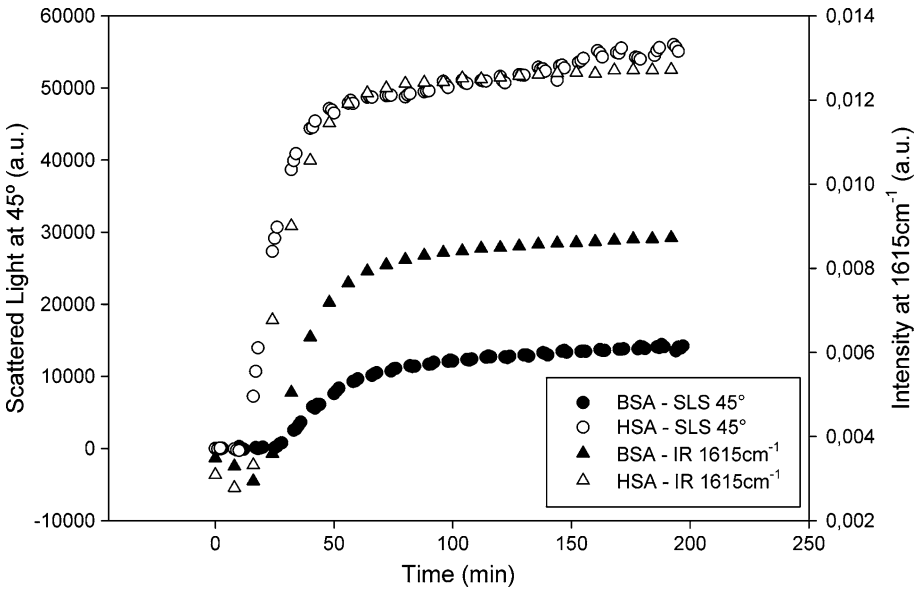

Fig. 6 Light-scattering measurement at 45° (*circles*) and time dependence of the FT-IR bands at 1,615 cm^{-1} (*triangles*) for BSA (*solid figures*) and HSA (*open figures*)

but the number of fibrils is higher, and so is the size of these particles, as can be seen from a plot of the dissymmetry, i.e., the ratio of the scattering intensities at 45° and 135° (Fig. 5c), which can be used as a coarse measure of size (Wyatt 1993).

Discussion

Despite the substantial progress made in the study of amyloid fibril properties, very little is known about their kinetics of formation. This fibrilization process gives rise to a common structure for most proteins, the so-called cross-β structure, characterized in the IR amide-I region by an intense band at low frequencies, because of the extended structures present in the fibril (Zandomeneghi et al. 2004). In this scenario, many aspects of the correlation between the structural and conformational changes of protein and the degree and type of aggregation remain open questions. The experimental approach usually used to monitor these aspects is based on such techniques as infrared spectroscopy or light scattering (Bouchard et al. 2000; Militello et al. 2004). However, there are no studies combining both methods under identical conditions and for the same sample. In this work we focused on development of a system enabling study of secondary structure and particle size during the formation of amyloid fibrils by use of FT-IR and SLS at the same time.

To prove the usefulness of this coupled system, we followed the amyloidogenesis process for two different serum albumins, human and bovine, which are both 66.4-kDa proteins with 88 % sequence identity. These albumins, non-pathological proteins under normal physiological conditions, are able to form fibers, with the advantage that the aggregation process can be controlled easily. Although there are no big differences between their polypeptide composition, the results obtained revealed different kinetics of amyloidogenesis, in agreement with the proposal that changes in polypeptide chains are one of the determinants of protein aggregation propensity (Cerdà-Costa et al. 2007; Chiti et al. 2003). These differences in the amino acid composition of human and bovine serum albumin can also be related to differences between two-dimensional correlation maps. Although the synchronous maps are very similar, because similar bands are indicative of changes of protein secondary structure, differences between the asynchronous maps indicate the process it is not the same in both aggregations. Nevertheless, the sequence of events for both albumins is very similar, with changes in the unordered structures enabling the appearance of the amyloid-related structures, followed by changes in the turns and the helical content of the proteins.

The differences between the fibril-formation processes are also clearly evident from the light-scattering data. Combination of FT-IR spectroscopy and static light scattering in the same device, using the same sample at the same time, enables a synoptic view of different processes and regions caused by the same structural alterations. In Fig. 5 it is clear that the differences between the fibrils are not only in the secondary structure of the final aggregate (Fig. 3b) but also in the size and number of fibrils formed. The light scattering intensity at 45° and 135° during the incubation, in combination with the results extracted from the time profile of the amyloid-related band at 1,615 cm^{-1}, confirm that the kinetics of amyloid formation also differ between human and bovine serum albumin, being slower in the latter.

Bovine and human serum albumin are very similar proteins that are affected differently by the conditions that give rise to an amyloid-like structure. BSA seems to be more stable against the perturbation, maintaining a greater amount of the native α-helix structure and producing less amyloid-like content, of smaller size, than HSA during the fibril-formation process.

Acknowledgments The authors would like to thank Ernst Winter and Viktor Schäfer, for excellent mechanical and electronic engineering, and Dr Georg Wille and Dr Vitali Vogel (all at the Institut für Biophysik) for valuable discussions. One of us (IdlA) is grateful to the Basque Government for a Postdoctoral Fellowship.

References

Arrondo JL, Muga A, Castresana J, Goñi FM (1993) Quantitative studies of the structure of proteins in solution by Fourier-transform infrared spectroscopy. Prog Biophys Mol Biol 59:23–56

Bouchard M, Zurdo J, Nettleton EJ et al (2000) Formation of insulin amyloid fibrils followed by FTIR simultaneously with CD and electron microscopy. Protein Sci 9:1960–1967

Bramanti E, Benedetti E (1996) Determination of the secondary structure of isomeric forms of human serum albumin by a particular frequency deconvolution procedure applied to Fourier-transform IR analysis. Biopolymers 38:639–653

Bucciantini M, Giannoni E, Chiti F et al (2002) Inherent toxicity of aggregates implies a common mechanism for protein misfolding diseases. Nature 416:507–511

Cerdà-Costa N, Esteras-Chopo A, Avilés FX et al (2007) Early kinetics of amyloid fibril formation reveals conformational reorganisation of initial aggregates. J Mol Biol 366:1351–1363

Cerdà-Costa N, De la Arada I, Avilés FX et al (2009) Influence of aggregation propensity and stability on amyloid fibril formation as studied by Fourier-transform infrared spectroscopy and two-dimensional COS analysis. Biochemistry 48:10582–10590

Charbonneau D, Beauregard M, Tajmir-Riahi H-A (2009) Structural analysis of human serum albumin complexes with cationic lipids. J Phys Chem B 113:1777–1784

Chiti F, Dobson CM (2006) Protein misfolding, functional amyloid, and human disease. Annu Rev Biochem 75:333–366

Chiti F, Stefani M, Taddei N et al (2003) Rationalization of the effects of mutations on peptide and protein aggregation rates. Nature 424:805–808

de la Arada I, Andraka N, Pacios MG, Arrondo JLR (2011) A conventional and 2DCOS infrared approach to the kinetics of protein misfolding. Curr Protein Pept Sci 12:181–187

Dobson CM (2003) Protein folding and misfolding. Nature 426: 884–890

Fabian H, Mäntele W, Werner M (2002) Infrared spectroscopy of proteins—Handbook of Vibrational Spectroscopy, pp 1–27

Froehlich E, Mandeville JS, Jennings CJ et al (2009) Dendrimers bind human serum albumin. J Phys Chem B 113:6986–6993

Gorinstein S, Caspi A, Rosen A et al (2002) Structure characterization of human serum proteins in solution and dry state. J Pept Res 59:71–78

He XM, Carter DC (1992) Atomic structure and chemistry of human serum albumin. Nature 358:209–215

Hill SE, Miti T, Richmond T, Muschol M (2011) Spatial extent of charge repulsion regulates assembly pathways for lysozyme amyloid fibrils. PLoS ONE 6:e18171

Huang H, Xie J, Chen H (2011) Adsorption behavior of human serum albumin on ATR crystal studied by in situ ATR/FTIR spectroscopy and two-dimensional correlation analysis. The Analyst 136:1747–1752

Jahn TR, Radford SE (2008) Folding versus aggregation: polypeptide conformations on competing pathways. Arch Biochem Biophys 469:100–117

Juárez J, Taboada P, Mosquera V (2009) Existence of different structural intermediates on the fibrillation pathway of human serum albumin. Biophys J 96:2353–2370

Kumar S, Udgaonkar J (2010) Mechanisms of amyloid fibril formation by proteins. Curr Sci 98:639–656

Lumry R, Smith EL, Glantz RR (1951) Kinetics of carboxypeptidase action. I. effect of various extrinsic factors on kinetic parameters. J Am Chem Soc 73:4330–4340

Militello V, Casarino C, Emanuele A et al (2004) Aggregation kinetics of bovine serum albumin studied by FTIR spectroscopy and light scattering. Biophys Chem 107:175–187

Noda I (2007) Two-dimensional correlation analysis useful for spectroscopy, chromatography, and other analytical measurements. Anal Sci 23:139–146

Noda I, Ozaki Y (2004) Two-dimensional correlation spectroscopy: applications in vibrational and optical spectroscopy, pp 1–310

Pearce F, Mackintosh S, Gerrard J (2007) Formation of amyloid-like fibrils by ovalbumin and related proteins under conditions relevant to food processing. J Agric Food Chem 55(2):318–322

Raussens V, Ruysschaert J-M, Goormaghtigh E (2004) Analysis of 1H/2H exchange kinetics using model infrared spectra. Appl Spectrosc 58:68–82

Sugio S, Kashima A, Mochizuki S et al (1999) Crystal structure of human serum albumin at 2.5 Å resolution. Protein Eng 12:439–446

Termine JD, Eanes ED, Ein D, Glenner GG (1972) Infrared spectroscopy of human amyloid fibrils and immunoglobulin proteins. Biopolymers 11:1103–1113

Tycko R (2004) Progress towards a molecular-level structural understanding of amyloid fibrils. Curr Opin Struct Biol 14:96–103

van de Hulst HC (1981) Light scattering by small particles. Dover Publications, Inc., New York, p 470

Witte T, Haller LA, Luttmann E et al (2007) Time resolved structure analysis of growing beta-amyloid fibers. J Struct Biol 159:71–81

Wyatt PJ (1993) Light scattering and the absolute characterization of macromolecules. Anal Chim Acta 272:1–40

Zandomeneghi G, Krebs MRH, McCammon MG, Fändrich M (2004) FTIR reveals structural differences between native beta-sheet proteins and amyloid fibrils. Protein Sci 13:3314–3321

Zurdo J, Guijarro JI, Dobson CM (2001) Preparation and characterization of purified amyloid fibrils. J Am Chem Soc 123:8141–8142